One-electron reduction product of biphosphinine derivative and of its Ni(0) complex: crystal structure, EPR/ENDOR and DFT investigations on (tmbp).- and [Ni(tmbp)2].-

Choua, Sylvie; Sidorenkova Cruz Gonzalez, Elena; Berclaz, Théo; Geoffroy, Michel; Rosa, Patrick; Mézailles, Nicolas; Ricard, Louis; Mathey, François; Le Floch, Pascal

How to cite

CHOUA, Sylvie et al. One-electron reduction product of biphosphinine derivative and of its Ni(0) complex: crystal structure, EPR/ENDOR and DFT investigations on (tmbp).- and [Ni(tmbp)2].-. In: Journal of the American Chemical Society, 2000, vol. 122, n° 49, p. 12227–12234. doi: 10.1021/ja002125+

This publication URL: https://archive-ouverte.unige.ch/unige:3604

Publication DOI: 10.1021/ja002125+

One-Electron Reduction Product of a Biphosphinine Derivative and of Its $Ni^{(0)}$ Complex: Crystal Structure, EPR/ENDOR, and DFT Investigations on $(tmbp)^{\bullet-}$ and $[Ni(tmbp)_2]^{\bullet-}$

Sylvie Choua,[†] Helena Sidorenkova,[†] Théo Berclaz,[†] Michel Geoffroy,*[,†] Patrick Rosa,[‡] Nicolas Mézailles,[‡] Louis Ricard,[‡] François Mathey,*[,‡] and Pascal Le Floch*[,‡]

Contribution from the Department of Physical Chemistry, 30 Quai Ernest Ansermet, University of Geneva, 1211 Geneva, Switzerland, and Laboratoire "Hétéroéléments et Coordination", UMR CNRS 7653, Ecole Polytechnique, 91128 Palaiseau Cedex, France

Received June 13, 2000

Abstract: The radical anion $(tmbp)^{\bullet-}$, where tmbp = 4,4′,5,5′-tetramethyl-2,2′-biphosphinine, was generated by reduction of tmbp on a potassium mirror. EPR/ENDOR spectra and DFT calculations show that, in contrast to the neutral species, this anion is planar and that the unpaired electron is mainly delocalized on the PCCP fragment with a large participation of the phosphorus p_π orbitals. This planar structure was confirmed by the first crystal structure of an anionic biphosphinine: [tmbp][Li(2.2.1)]. Reduction of $[Ni(tmbp)_2]$ led to the 19-electron complex whose **g** and ^{31}P hyperfine tensors were obtained from EPR in liquid and frozen solutions. These results, together with DFT calculations on $[Ni(bp)_2]$ and $[Ni(bp)_2]^{\bullet-}$, indicate that, by accepting an extra electron, the neutral nickel complex distorts toward a more planar geometry and that the dihedral angle between the two phosphinine rings of each ligand slightly increases. In the reduced Ni complex, the unpaired electron is mainly delocalized on the ligands, in a molecular orbital which retains the characteristics of the SOMO found for the reduced isolated ligand. A charge decomposition analysis (CDA) shows that, in $[Ni(bp)_2]$, metal−ligand back-donation strongly contributes to the metal−ligand bonding.

Introduction

Electron transfer in transition-metal complexes is currently a very active research field with numerous applications in catalysis, molecular electronics, and materials science.[1] In this context, a good understanding of structural modifications induced by these electron-transfer processes is of utmost importance. Since ligands' properties are generally essential to explain these modifications (e.g., ability to accommodate extra electrons, flexibility...), the determination of the structural changes in the ligand alone is a prerequisite to the study of geometrical distortions in the full complex.

Nitrogen-containing molecules with a low-lying antibonding π^* orbital have been widely used for decades as chelating agents.[2,3] This is particularly the case for 2,2′-bipyridine (bipy) whose anionic structures were resolved only quite recently.[4] Recent developments in the chemistry of low-coordinated phosphorus compounds[5−7] has led to the discovery of new ligands whose coordination properties are expected to appreciably differ from those of their nitrogen homologues. Due to their low-lying π^* orbitals, biphosphinines,[8−10] the phosphorus analogues of bipyridines, seem to be very appropriate for the stabilization of electron-rich metal centers.[11]

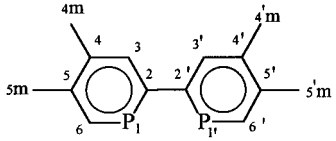

***cis*-tmbp**

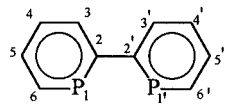

***cis*-bp**

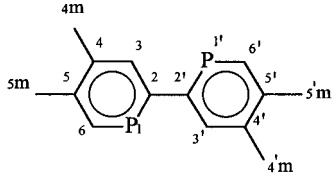

***trans*-tmbp**

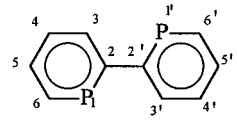

***trans*-bp**

In the present study, we report on the crystal structure of the first crystallized Li salt of the 4,4′,5,5′-tetramethyl-2,2′-biphos-

[†] University of Geneva.
[‡] Ecole Polytechnique.

(1) Astruc, D. *Electron Transfer and Radical Processes in Transition-Metal Chemistry*; Wiley-VCH: New York, 1995.
(2) Vlcek, A. *Coord. Chem. Rev.* **1982**, *43*, 39.
(3) Juris, A.; Balzani, F.; Campagna, S.; Belser, P.; Von Zelewsky, A. *Coord. Chem. Rev.* **1988**, *84*, 85.
(4) (a) Bock, H.; Lehn, J.-M.; Pauls, J.; Holl, S.; Krenzel, V. *Angew. Chem., Int. Ed.Angew. Chem., Int. Ed.* **1999**, *38*, 952. (b) Echegoyen, L.; DeCian, A.; Lehn, J.-M. *Angew. Chem., Int. Ed. Engl.* **1991**, *30*, 838. (c) Bock, H.; Havlas, Z.; Hess, D.; Näther, C. *Angew. Chem., Int. Ed.* **1998**, *37*, 502. (d) Fedushkin, I. G.; Petrovskaya, T. V.; Girgsdies, F.; Köhn R. D.; Bochkarev, M. N.; Schumann, H. *Angew. Chem., Int. Ed.* **1999**, *38*, 2262.
(5) (a) *Multiple Bonds and Low Coordination in Phosphorus Chemistry*; Regitz, M., Scherer, O. J., Eds.; Georg Thieme Verlag: Stuttgart, 1990. (b) Dillon, K. B.; Mathey, F.; Nixon J. F. *Phosphorus: the Carbon Copy*; Wiley: Chichester, 1998.
(6) Avarvari, N.; Mézailles, N.; Ricard, L.; Le Floch, P.; Mathey, F. *Science* **1998**, *280*, 1587.
(7) Jouaiti, A.; Geoffroy, M.; Terron, G.; Bernardinelli, G. *J. Am. Chem. Soc.* **1995**, *117*, 2251.
(8) Le Floch, P.; Carmichael, D.; Ricard, L.; Mathey, F.; Jutand, A.; Amatore, C. *Organometallics* **1992**, *11*, 2475.
(9) Mathey, F.; Le Floch, P. *Chem. Ber.* **1996**, *129*, 263.
(10) Rosa, P., Ricard, L.; Mathey, F.; Le Floch, P. *Organometallics* **1999**, *18*, 3348.

10.1021/ja002125+ CCC: $19.00
Published on Web 11/23/2000

phinine (tmbp) and discuss the electronic structure of the anion radical $(tmbp)^{\bullet-}$ as obtained from EPR/ENDOR spectroscopy and density functional theory (DFT) calculations. In particular, we determine the participation of the heteroatom to the single occupied molecular orbital (SOMO). These MO coefficients are highly important in the context of complexation since they characterize the junction between the π acceptor ligand and the low-valent metal[12] and have been invoked for explaining numerous properties of nitrogen-containing ligands.[13] We can, now, show how the SOMO is affected by coordination to a metal and assess structural and electronic changes resulting from spin delocalization on the biphosphinine ligands; for this purpose we have generated the 19-electron biphosphinine complex $[Ni(tmbp)_2]^{\bullet-}$ and determined its spin repartition from its liquid- and solid-phase EPR spectra. These results are discussed in the light of DFT calculations performed on the complex $[Ni(bp)_2]$ and its radical anion.

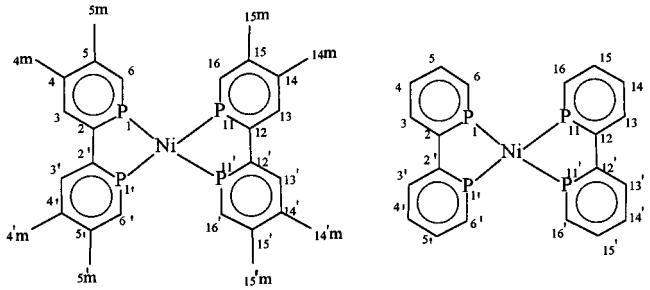

Experimental Section

Preparation of [tmbp][Li(2.2.1)]. Biphosphinine (25 mg, 0.1 mmol) and Kryptofix (2.2.1) (29 mg, 0.10 mmol) in DME (6 mL) were reacted with lithium naphthalene (0.11 mmol) at room temperature for 2 h. A part of the solution (2 mL) was then transferred into a glass tube which was sealed under vacuum. Crystals of [tmbp][Li(2.2.1)], which are highly oxygen- and moisture-sensitive, were obtained after 5 days standing at − 18 °C. Crystallographic data and experimental parameters are given in Table 1.

Compounds. tmbp[14] and $[Ni(tmbp)]_2$ were synthesized following the method reported in ref 11.[11]

EPR/ENDOR. The spectra were recorded on a Bruker ESP 300 spectrometer equipped with a variable temperature attachment and an ENI 500 W power supply. Freshly distilled solvents were used for the preparation of all samples, and solutions were carefully degassed. Electrochemical reductions of the samples (5×10^{-3} M) were carried out in the EPR cavity using a quartz cell and platinum electrodes. Bu_4NPF_6 (0.2 M) was used as an electrolyte. Chemical reductions were performed under vacuum by reacting a solution of the substrate in DME on a potassium mirror.

Optimizations and simulations of the frozen solution EPR spectra were performed with a program,[15] based on the algorithm of Levenberg−Marquardt, which compares the position of the experimental resonance lines with those calculated by second-order perturbation theory.

DFT Calculations. Calculations were performed on a Hewlett-Packard Convex Exemplar and on a Silicon Graphics workstation with the Gaussian 98 package.[16] Geometries were optimized with spin-unrestricted DFT calculations using B3LYP functional.[17] The optimized structures of the ligands and Ni complexes were characterized by harmonic frequency analysis as minima (all frequencies real). The MO were represented with the Molekel program[18] by running a single-point restricted-DFT calculation at the optimized geometry.

The 6-31G* and 6-31+G* standard basis sets were used for the calculations on the neutral (bp and tmbp) and anionic ($bp^{\bullet-}$ and $tmbp^{\bullet-}$) ligands, respectively. DFT calculations on $[Ni(bp)_2]$ were carried out using the 6-31G* basis set for the ligand's atoms, and either the LANL2DZ[19] basis set or the Stevens−Basch−Krauss ECP triple-split basis (SBK)[20] for nickel. Similar basis set choices were made for the calculations on the anion $[Ni(bp)_2]^{\bullet-}$, except that the 6-31G* basis was replaced by the 6-31+G* basis set. Optimizations of both the neutral and anionic complexes have been performed, assuming D_2 symmetry. The results reported in this study correspond to the SBK basis set for Ni, the other results are given as Supporting Information.

Charge decomposition analysis[21] (CDA) was performed using the program CDA 2.1.[22] These calculations were performed for the geometry which was optimized with the SBK basis set for Ni; however,

Table 1. Crystallographic Data and Experimental Parameters for the Structure of [tmbp] [Li(2.2.1)]

mol formula	$C_{30}H_{48}LiN_2O_5P_2$
mol wt	585.58
crystal description (habit/size (mm))	deep purple cube $0.20 \times 0.20 \times 0.20$
crystal system	triclinic
space group	*P*-1
a (Å)	11.5316(6)
b (Å)	11.5497(5)
c (Å)	13.0148(4)
α (deg)	74.998(3)
β (deg)	74.883(3)
γ (deg)	72.182(2)
V (Å^3)	1562.62(12)
Z	2
D (g/cm^3)	1.245
F(000)	630
μ (cm^{-1})	0.179
T (K)	150.0(1)
max Θ (deg)	30.02
hkl ranges	−13 16; −14 16; −14 18
no. of reflections measured	11139
no. of independent reflections	8644
no. of reflections used	7067
R_{int}	0.0348
refinement type	F^2
hydrogen atoms	mixed
no. of parameters refined	365
reflection/parameter ratio	19
wR2	0.1356
R1	0.0401
criterion	$>2\sigma(I)$
GOF	1.102
diff peak/hole (eÅ^3)	0.449(0.135)/−0.445(0.135)

(11) (a) Le Floch, P.; Carmichel, D.; Ricard, L.; Mathey, F. *J. Am. Chem. Soc.* **1991**, *113*, 667. (b) Le Floch, P.; Ricard, L.; Mathey, F.; Jutand, A.; Amatore, C. *Inorg. Chem.* **1995**, *34*, 11.

(12) Klein, A.; Kaim, W.; Waldhör, E.; Hausen, H.-D. *J. Chem. Soc., Perkin Trans. 2* **1995**, 2121.

(13) Ernst, S.; Vogler, C.; Klein, A.; Kaim. W. *Inorg. Chem.* **1996**, *35*, 1295 and references therein.

(14) Rosa, P.; Mézailles, N.; Mathey, F.; Le Floch, P. *J. Org. Chem.* **1998**, *63*, 4826.

(15) Soulié, E.; Berclaz, T.; Geoffroy, M. *AIP Conference Proceedings 330, Computational Chemistry*, **1996**, 627; Bernardi, F., Rivail, J.-L., Eds.

(16) Frisch, M. J.; Trucks, G. W.; Schlegel, H. B.; Scuseria, G. E.; Robb, M. A.; Cheeseman, J. R.; Zakrzewski, V. G.; Montgomery, J. A., Jr.; Stratmann, R. E.; Burant, J. C.; Dapprich, S.; Millam, J. M.; Daniels, A. D.; Kudin, K. N.; Strain, M. C.; Farkas, O.; Tomasi, J.; Barone, V.; Cossi, M.; Cammi, R.; Mennucci, B.; Pomelli, C.; Adamo, C.; Clifford, S.; Ochterski, J.; Petersson, G. A.; Ayala, P. Y.; Cui, Q.; Morokuma, K.; Malick, D. K.; Rabuck, A. D.; Raghavachari, K.; Foresman, J. B.; Cioslowski, J.; Ortiz, J. V.; Stefanov, B. B.; Liu, G.; Liashenko, A.; Piskorz, P.; Komaromi, I..; Gomperts, R.; Martin, R. L.; Fox, D. J.; Keith, T.; Al-Laham, M. A.; Peng, C. Y.; Nanayakkara, A.; Gonzalez, C.; Challacombe, M.; Gill, P. M. W.; Johnson, B. G.; Chen, W.; Wong, M. W.; Andres, J. L.; Head-Gordon, M.; Replogle, E. S.; Pople, J. A. *Gaussian 98*, revision A.7; Gaussian, Inc.: Pittsburgh, PA, 1998.

(17) Becke, A. D. *J. Chem. Phys.* **1993**, *98*, 5648.

(18) Flukiger, P. Development of Molecular Graphics Package MOLEKEL. Ph.D. Thesis, University of Geneva, Switzerland, 1992.

(19) Hay, P. J.; Wadt, W. R. *J. Chem. Phys.* **1985**, *82*, 270.

(20) Stevens, W.; Basch, H.; Krauss, J. *J. Chem. Phys.* **1984**, *81*, 6026.

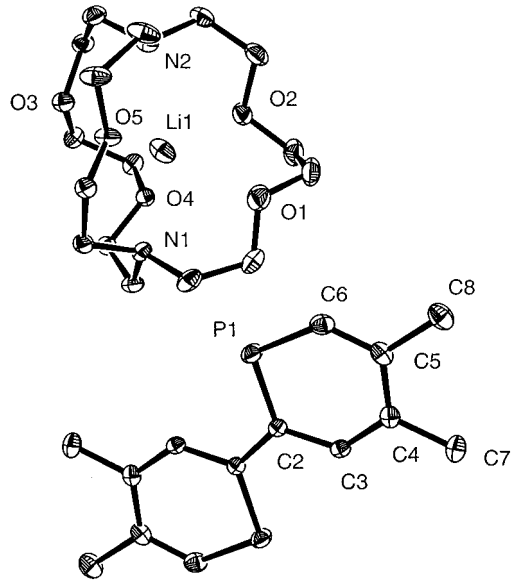

Figure 1. ORTEP drawing of one molecule of [tmbp][Li(2.2.1)]. Selected bond distances (Å) and angles (deg): P1−C6, 1.741(1); C6−C5, 1.379(2); C5−C4, 1.429(2); C4−C3, 1.381(2); C3−C2, 1.429(2); C2−P1, 1.784(1); C2−C2′, 1.440(2); C2−P1−C6, 100.80(6), C6−C5−C4, 120.4(1); C5−C4−C3, 121.9(1), C4−C3−C2, 128.1(1), C3−C2−P1, 119.7(1), P1−C2−C2′, 120.5(1).

to facilitate the comparison with previous results, the CDA program was run, for the nickel, with the LANL2DZ basis set[23] modified as described by Petz et al.[24,25]

X-ray Structure Determination. Data were collected on a Nonius Kappa CCD diffractometer using an Mo Kα (λ = 0.71070 Å) X-ray source and a graphite monochromator. Experimental details are described in Table 1. The crystal structure was solved using SIR 97[26] and Shelxl-97.[27] ORTEP drawings were made using ORTEP III for Windows.[28]

Results

1. The tmbp Radical Anion. a. Synthesis and Crystal Structure of the tmbp Radical Anion. Reduction of tmbp was carried out using naphthalene lithium as reducing agent. To avoid the formation of a polymeric ion-pair structure, this reduction was conducted in the presence of 1 equiv of Kryptofix (2.2.1). Suitable crystals of [tmbp][Li(2.2.1)] were obtained after keeping the crude solution at −18 °C for 5 days in a sealed tube.

As expected, a monomeric ion-pair structure was obtained. An ORTEP view of [tmbp][Li(2.2.1)] is shown in Figure 1. The structure of [tmbp][Li(2.2.1)] consists of a cryptated $[Li(2.2.1)]^+$ unit and a $(tmbp)^{\bullet-}$ anion, which adopts a perfectly planar *trans* conformation. This planarity indicates a delocalization of the charge on the two phosphinine rings. Additional significant geometrical features are given by the bond lengths which obviously strongly differ from those recorded for the free tmbp. Significant lengthening of the P═C bond lengths (for internal P═C bonds: 1.784(1) Å versus 1.731(4)−1.740(5) Å in the free *trans*-tmbp) and a shortening of the C−C bridge connection (1.440(2) Å versus 1.484(6) Å in the free *trans*-tmbp) are observed. Accordingly, the aromaticity within both rings is slightly disrupted as shown by two C═C bond lengths which are partly localized. Thus, whereas C5−C6 (1.379(2) Å versus 1.396(4) Å in *trans*-tmbp) and C3−C4 (1.381(2) Å versus 1.380(6) Å) are close to those of the free ligand, C4−C5 (1.429(2) Å versus 1.396(4)) and C2−C3 (1.429(2) Å versus 1.401(4) Å) appear to be slightly lengthened. On the other hand, bond angles are not significantly modified (for example: C2−P1−C6 at 100.80(6) Å in $tmbp^{\bullet-}$ versus 100.7(2) Å in the free *trans*-tmbp).

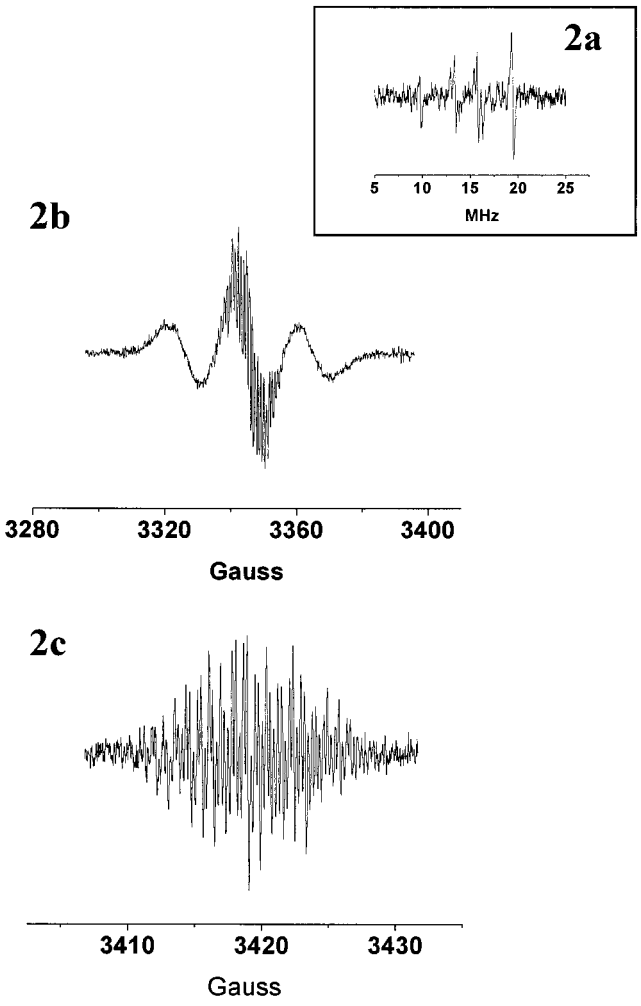

Figure 2. (a) ^{1}H-ENDOR spectrum obtained at 185 K after reduction of tmbp. (b) EPR spectrum obtained with a solution of tmbp in DME after reaction on a potassium mirror (klystron frequency = 9.3678 GHz). (c) Central part of the EPR spectrum (klystron frequency = 9.5791 GHz).

b. EPR/ENDOR Spectra of the Reduction Product of tmbp. Consistent with the previous report on the reversible one-electron reduction of tmbp at −1.86 V versus SCE (in DMF), we could detect the EPR signals caused by the electrochemical reduction of a DME solution of this biphosphinine in situ in the EPR cavity at 220 K. Moreover, a solution of tmbp in DME turned red when passed on a potassium mirror at 200 K and led to spectra similar to those obtained by electrochemical

(21) Dapprich, S.; Frenking, G. *J. Phys. Chem.* **1995**, *99*, 9382.
(22) Dapprich, S.; Frenking, G. CDA 2.1, Phillipps-Universität: Marburg, 1994.
(23) Hay, P. J.; Wadt, W. R. *J. Chem. Phys.* **1985**, *98*, 5648.
(24) Petz, W.; Weller, F.; Uddin, J.; Frenking, G. *Organometallics* **1999**, *18*, 619.
(25) Frenking, G.; Antes, I.; Böhme, M.; Dapprich, S.; Ehlers, A. W.; Jonas, V.; Neuhaus, A.; Otto, M.; Stegmann, R.; Veldkamp, A.; Vyboishchikov, S. F. In *Reviews in Computational Chemistry*; Lipkowitz, K. B., Boyd, D. B., Eds.; VCH: New York, 1996; Vol. 8, pp 63−144.
(26) Altomare, A.; Burla, M. C.; Camalli, M.; Cascarano, G.; Giacovazzo, C.; Guagliardi, A.; Moliterni, A. G. G.; Polidori, G.; Spagna, R. *SIR97*, an integrated package of computer programs for the solution and refinement of crystal structures using single-crystal data, 1999.
(27) Sheldrick, G. M. *SHELXL-97;* Universität Göttingen: Göttingen, Germany, 1997.
(28) Farrugia, L. J. ORTEP-3 program; Department of Chemistry: University of Glasgow, 1997.

Table 2. EPR/ENDOR Parameters for the $(tmbp)^{\bullet-}$ Radical Anion

liquid solution						frozen solution					
								Hyperfine coupling ($^{31}P_1$, $^{31}P_{1'}$), (MHz)			
g	isotropic coupling constants (MHz)							total		anisotropic	
	$^{31}P_1$, $^{31}P_{1'}$	^1H (C_6,$C_{6'}$)	^1H (C_3,$C_{3'}$)	^1H (C_{4m},$C_{4'm}$)	^1H (C_{5m},$C_{5'm}$)	$g_{\|\|}$	$g_\perp$	$T_{\|\|}$	$T_\perp$	$\tau_{\|\|}$	$\tau_\perp$
2.0019	59	1.6	2.3	3.1	9.6	2.0027	2.005	204.4	−14	145.6	−72.8

Table 3. Experimental and Calculated (DFT) Geometries for tmbp and for Its Radical Anion

	bond lengths (Å)			bond angles (deg)			torsion angles (deg)[a]		
	C_6-P_1	P_1-C_2	$C_2-C_{2'}$	$C_6P_1C_2$	$P_1C_2C_{2'}$	$P_1C_2C_3$	$C_6P_1C_2C_3$	$\xi = P_1C_2C_{2'}P_{1'}$	$C_2C_{2'}P_{1'}C_{6'}$
					Neutral				
cis-**tmbp** (crystal)	1.716	1.736	1.490	100.2	115.6	123.2	4.3	46.6	172.7
trans-**tmbp** (crystal)	1.716	1.731	1.484	100.7	118.6	121.4	4.94	148.9	177.3
cis-**bp** (DFT)	1.745	1.768	1.487	100.8	117.8	122.9	1.1	47.5	179.5
trans-**bp** (DFT)	1.743	1.770	1.488	101.1	117.6	119.6	1.2	134.8	179.7
					Anion				
trans-**tmbp**$^{\bullet-}$ (crystal)	1.740	1.784	1.440	100.8	120.4	119.6	3.1	180.0	177.3
cis-**bp**$^{\bullet-}$ (DFT)	1.766	1.815	1.451	101.1	118.5	119.7	1.5	9.0	179.4
trans-**bp**$^{\bullet-}$ (DFT)	1.759	1.822	1.444	101.6	121.8	119.1	0.0	180.0	180.0
cis-**tmbp**$^{\bullet-}$ (DFT)	1.763	1.813	1.454	100.4	118.5	119.2	0.0	0.0	180.0
trans-**tmbp**$^{\bullet-}$ (DFT)	1.755	1.815	1.445	100.9	121.3	118.6	0.0	179.9	180.0

[a] Absolute value

Table 4. DFT Calculated Hyperfine Couplings (MHz) for the Radical Anions $(bp)^{\bullet-}$ and $(tmbp)^{\bullet-}$

	Isotropic coupling constants							anisotropic coupling ($^{31}P_1$,$^{31}P_{1'}$)		
	$^{31}P_1$, $^{31}P_{1'}$	^1H (C_6,$C_{6'}$)	^1H (C_3,$C_{3'}$)	^1H (C_4,$C_{4'}$)	^1H (C_5,$C_{5'}$)	CH_3[a] (4m, 4′m)	CH_3[a] (5m, 5′m)	$\tau_{\|\|}$	$\tau_{\perp1}$	$\tau_{\perp2}$
(*cis*-**bp**)$^{\bullet-}$	32.1	1.2	0.28	4.45	7.53			160.1	−84.0	−76.1
(*trans*-**bp**)$^{\bullet-}$	38.3	2.66	2.6	2.0	9.89			153.3	−79.8	−73.5
(*cis*-**tmbp**)$^{\bullet-}$	30.8	0.37	0.19			5.18	6.28	156.2	−81.9	−74.3
(*trans*-**tmbp**)$^{\bullet-}$	36.7	2.36	2.57			2.58	8.68	149.5	−77.9	−71.6
average (*cis* + *trans*) (**tmbp**)$^{\bullet-}$	33.7	1.36	1.38			3.88	7.48			

[a] After averaging of the three proton couplings.

reduction. These spectra are characterized by three main lines whose relative intensities considerably vary with temperature: whereas the lateral signals are hardly detected below 220 K, the intensity distribution is almost 1−2−1 above 250 K. This effect is probably due to line-broadening caused by a partial averaging of the **g** and dipolar hyperfine tensors, it explains why the additional hyperfine structure is considerably better resolved on the central line than on the sidebands. Furthermore, since the highest resolution is obtained after chemical reduction, we will concentrate on the spectra recorded after reaction of tmbp with a potassium mirror.

The ^1H ENDOR spectrum recorded at 185 K with a solution of tmbp in DME after reaction on a potassium mirror, is shown in Figure 2a, while the EPR spectrum is shown in Figure 2b. The central part of this latter spectrum, shown in Figure 2c, could be very satisfactorily simulated by using the ^1H coupling constants obtained from the ENDOR spectrum. These isotropic coupling constants, as well as the number of associated protons, are shown in Table 2, together with the two identical ^{31}P hyperfine constants measured on the EPR spectrum.

The frozen solution EPR spectrum was obtained at 110 K. It was easily simulated by assuming two aligned ^{31}P hyperfine tensors. The symmetry of these tensors is axial; the perpendicular values were determined from the parallel component (directly measured on the low-temperature spectrum) and from the isotropic constants (measured on the fluid solution spectrum). These values are also given in Table 2.

c. DFT Structure of the Biphosphinine-Containing Systems. Optimizations of the structure of neutral bp led to two minimum energy conformations which correspond to the *cis*- and *trans*-isomers, respectively. In the *cis*-isomer the torsion angle ξ ($\xi = P_1C_2C_{2'}P_{1'}$) between the two phosphinine planes is close to 45°, while it is equal to ∼135° in the *trans*-isomer. These two isomers have almost the same energy ($E_{trans} - E_{cis} = -0.54$ kcal mol^{-1}). Some geometrical parameters are given in Table 3 together with those previously obtained from the crystal structures of *cis*- and *trans*-tmbp. Although the ξ angle calculated for *trans*-bp (134.8°) is found to be slightly smaller than that obtained from the crystal structure of *trans*-tmbp (148.9°), the accord between experimental (tmbp) and calculated (bp) geometries remains quite satisfactory.

DFT optimized parameters for the *cis*- and *trans*-isomers of both radical anions $(bp)^{\bullet-}$ and $(tmbp)^{\bullet-}$ are shown in Table 3. It is clear that the presence of the methyl groups does not appreciably affect the structure of the radical anion. (*trans*-tmbp)$^{\bullet-}$ is found to be slightly more stable than the *cis*-isomer $E_{trans} - E_{cis} = -1.6$ kcal mol^{-1}. As shown in Table 3, the experimental geometry of (*trans*-tmbp)$^{\bullet-}$ obtained from the crystal structure of [tmbp][Li(2.2.1)] is in very good accord with the DFT optimized structure of (*trans*-tmbp)$^{\bullet-}$.

The ^1H and ^{31}P isotropic coupling constants as well as the diagonalized ^{31}P hyperfine tensors calculated for *cis*- and *trans*-isomers of both $(bp)^{\bullet-}$ and $(tmbp)^{\bullet-}$ are given in Table 4. Since the methyl groups are expected to rapidly rotate around the C−C bond, the reported ^1H isotropic coupling of the methyl is the average value of the three protons. For each isomer, the two $^{31}P-\tau_{\|}$ eigenvectors are aligned.

The calculated ^{31}P couplings are not very sensitive to the *cis*/

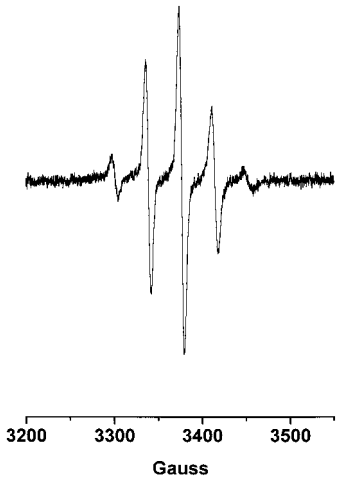

Figure 3. EPR spectrum obtained at room temperature with a solution of [Ni(tmbp)$_2$] after electrochemical reduction.

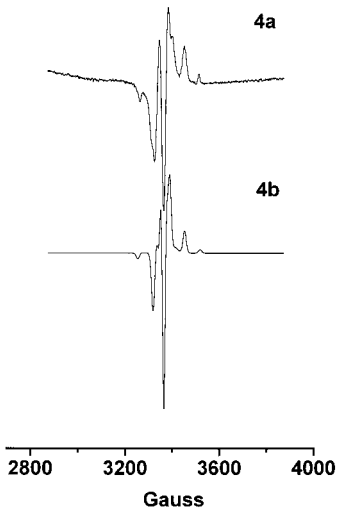

Figure 4. (a) EPR spectrum obtained at 110 K with a solution of [Ni(tmbp)$_2$] after electrochemical reduction. (b) Simulated spectrum obtained with the hyperfine tensors calculated by DFT.

trans isomerism; they suggest that the contributions of these two isomers cannot be separated on a frozen solution spectrum.

2. The [Ni(tmbp)$_2$] Complex. a. EPR Spectra of the Reduction Product of [Ni(tmbp)$_2$]. As previously reported, cyclic voltammetry of [Ni(tmbp)$_2$] in THF presents two reversible one-electron reduction waves at −1.64 and −1.89 V (vs SCE), respectively. The electrochemical reduction of a solution of [Ni(tmbp)$_2$] in THF in the EPR cavity at room temperature, leads to the spectrum shown in Figure 3. This spectrum is characterized by a hyperfine coupling of 103 MHz with four equivalent ^{31}P nuclei. The asymmetric distribution of intensities is probably due to the relative orientation of the anisotropic **g** and ^{31}P hyperfine tensors; this is confirmed by the temperature dependence of the spectra between 300 and 200 K: the asymmetry increases by diminishing the reorientation rate of the complex. The frozen solution spectrum obtained at 110 K is rather complex (Figure 4a) and could not be satisfactory simulated with four mutually aligned axial ^{31}P tensors. As explained below, the various hyperfine tensors (Table 5) as well as their mutual orientations could be determined owing to DFT calculations.

b. DFT Calculations. The above-mentioned results show, both in tmbp and bp, that the presence of the methyl groups has only little effect on the optimized structure. Therefore, we carried out the DFT calculation on the [Ni(bp)$_2$] complex. The resulting geometrical parameters are reported in Table 6 together with those obtained from the crystal structure of [Ni(tmbp)$_2$]. The dihedral angle φ is formed by the two planes $P_1NiP_{1'}$ and $P_{11}NiP_{11'}$ and characterizes the coordination geometry ($\varphi = 0$: planar; $\varphi = 90°$: tetrahedral).

The calculated ^{31}P Fermi contact coupling together with the eigenvalues and eigenvectors of the dipolar hyperfine tensor are reported in Table 5. The anisotropic hyperfine interaction for ^{61}Ni was also calculated ($\tau_1 = 28.4$, $\tau_2 = -1.7$, $\tau_3 = -26.7$ MHz) but, due to the low natural abundance of this isotope (1.1%) the corresponding signals cannot be detected on the spectrum.

The frozen solution spectrum was simulated by means of a program which optimized both the **g** tensor and the four ^{31}P coupling tensors. In this procedure the initial values of the four nondiagonalized ^{31}P hyperfine tensors were those previously calculated by DFT. The simulated spectrum, shown in Figure 4b**,** is in very good accord with the experimental one. The ^{31}P hyperfine tensors were not modified by the optimization process.

Discussion

(a) Ligand Structure. DFT calculations clearly indicate (Table 3) that the bp system becomes planar when it undergoes a one-electron reduction: the absolute value of the dihedral angle ξ between the two phosphinine rings decreases from 46° to 9° for the *cis*-isomer, and increases from 135° to 180° for the *trans*-isomer. As shown in Table 3,the same effect is observed by comparing the crystal structure of *trans*-tmbp with that of *trans*-[tmbp][Li(2.2.1)].

Since NMR showed that no restriction occurs in the rotation around the central C−C bond in neutral tmbp, and since the DFT energies of the *cis*- and *trans*-isomers of (tmbp)•⁻ are almost equal, the hyperfine constants measured in liquid solution correspond to the *average* values for the two isomers. Following, the proton coupling constants measured by ENDOR (Table 2) are in reasonable accord with the values calculated by DFT (Table 4). As often remarked,[29] the agreement between the experimental and DFT ^{31}P isotropic couplings is only modest. However, as shown in Tables 2 and 4, the accord on the ^{31}P dipolar couplings is very satisfactory: the eigenvalues are similar, and the $\tau_{||}$ eigenvectors of the two phosphorus couplings of each isomer are parallel. Direct information on the phosphorus participation to the SOMO of (tmbp)•⁻ can be obtained from the EPR/ENDOR spectra by comparing the measured ^{31}P coupling with the atomic constants:[30] $^{31}P-\tau_{||}$ leads to a spin density of 0.20 in a p orbital of each phosphorus atom; the small ^{31}P Fermi contact interaction ($\rho_s = 0.004$) is probably due to inner shell polarization. These results are consistent with the SOMO calculated by DFT and which is represented in Figure 5 together with a scheme of the various frontier orbitals. This SOMO is antibonding between the phosphorus and the adjacent central carbon (e.g., P1−C2) and bonding between the two central carbons C2 and C2′. This is in accord with the decrease of the C2−C2′ bond length and the increase of the internal P═C bonds which accompany the reduction of tmbp. As shown in Table 3, DFT calculations predict very well the bond lengths modifications observed on the crystal structures of tmbp and (tmbp)•⁻. The situation is reversed for the highest doubly occupied MO (HDOMO): in this case the MO is antibonding between C2 and C2′. As shown in Figure 5, the two higher-

(29) Chentit, M.; Sidorenkova, H.; Geoffroy, M.; Ellinger, Y. *J. Phys. Chem.* **1998**, *102*, 10469.

(30) Morton, J. R.; Preston, K. F. *J. Magn. Reson.* **1978**, *30*, 577.

Table 5. Hyperfine Parameters for $[Ni(bp)_2]^{\bullet-}$(DFT calculated) and $[Ni(tmbp)_2]^{\bullet-}$ (experimental)

^{31}P-hyperfine interaction (MHz) (4P)							*g*- values	
$[Ni(bp)_2]^-$ (calculated)[a]						$[Ni(tmbp)_2]^{\bullet-}$	$[Ni(tmbp)_2]^{\bullet-}$	
			direction cosines[b]			liquid solution	liquid	solid
total coupling	isotropic A_{iso}	anisotropic τ	λ	μ	ν	isotropic A_{iso}	$g_{averaged}$	**g**-tensor
$T_{\|\|}$: 183 $T_{\perp1}$: 45 $T_{\perp2}$: 51	93	$\tau_{\|\|} = 90$ $\tau_{\perp1} = -48$ $\tau_{\perp2} = -42$	0.3304	0.0972	0.9388	103	1.993	$g_{\|\|} = 1.990$ $g_{\perp} = 2.0015$

[a] These values obtained from DFT calculations on $[Ni(bp)_2]^{\bullet-}$ lead to a satisfactory simulation of the EPR spectrum obtained with a frozen solution of $[Ni(tmbp)_2]^{\bullet-}$. [b] The direction cosines of the three other $^{31}P-\tau'_{\|}$ eigenvectors are given by: $-\lambda, \mu, \nu$; $\lambda, -\mu, \nu$; $\lambda, \mu, -\nu$.

Table 6. Calculated and Experimental Geometrical Parameters for Neutral and Negatively Charged Ni Complexes

parameter	$[Ni(tmbp)_2]$ (crystal)	$[Ni(bp)_2]$ (DFT)	$[Ni(bp)_2]^{\bullet-}$ (DFT)
P_1-C_2	1.748	1.771	1.797
$C_2-C_{2'}$	1.466	1.470	1.443
C_2-C_3	1.396	1.402	1.411
C_5-C_6	1.395	1.391	1.385
$Ni-P_1$	2.140	2.180	2.194
angle P_1NiP_{11}	113.97	112.95	110.24
angle $P_1NiP_{11'}$	132.51	133.38	137.73
angle $P_1NiP_{1'}$	85.20	85.60	85.06
dihedral angle $P_{1'}C_{2'}C_2P_1$	−7.96	−13.39	−20.47
interplane angle φ (Ni coordination)	74.40	71.50	64.20

energy orbitals of the anion (SOMO and HDOMO) differ from the two higher-energy orbitals of the neutral species (LUMO and HOMO) only by the dihedral angle between the two phosphinine rings. However, in contrast to the third orbital of neutral bp which involves P−C and C−C π bonds, the third orbital of the anion $(MO)_{lp^*}$ mainly results from an antisymmetric combination of the two phosphorus lone pairs. The corresponding $(MO)_{lp^*}$ in the neutral species appears only in fifth rank from the LUMO ($E_{LUMO} - E_{(MO)lp^*} = 5.32$ eV). This increase in energy of $(MO)_{lp^*}$ for the anion ($E_{SOMO} - E_{(MO)lp^*} = 3.4$ eV) is consistent with the anion planarity which enforces the repulsive interaction between the two lone pairs; it suggests a more pronounced σ-donor character for $(bp)^{\bullet-}$ than for bp.

(b) Structure of the [Ni(tmbp)$_2$] Complex. As expected, by chelating nickel, the biphosphinine system becomes almost planar: the PCCP dihedral angle decreases from ∼45° to ∼8° in $[Ni(tmbp)_2]$ (crystal structure) and to ∼13° in $[Ni(bp)_2]$ (DFT calculations). As usual, the coordination of the metal atom can be characterized by the angle φ between the normals to the $P_1NiP_{1'}$ and $P_{11}NiP_{11'}$ planes. Whereas this angle is equal to 74° for $[Ni^{(0)}(tmbp)_2]$, the DFT calculations predict that the Ni coordination is appreciably less tetrahedral for the reduced complex ($\varphi = 64°$). As shown in Table 6, this change is accompanied, in $[Ni(bp)_2]^{\bullet-}$, by an increase of 7° in the PCCP torsion angle (ξ) of each ligand. These characteristics of the complex's geometry are directly revealed by the mutual orientations of the ^{31}P coupling tensors. The symmetry of these calculated tensors is axial with the "parallel" eigenvector oriented almost perpendicular to the plane of the corresponding phosphinine ring (e.g., the angle between the normal to the C2P1C6 and $\tau_{\|}-P1$ eigenvector is equal to 5°) and the angle between the two $^{31}P-\tau_{\|}$ eigenvectors of the same ligand is equal to 26.8°. The angles between the $^{31}P-\tau_{\|}$ eigenvectors of two different ligands are equal to 19.9 (e.g., $\tau_{\|}-P1$, $\tau_{\|}-P11$) and 33.7° (e.g., $\tau_{\|}-P1$, $\tau_{\|}-P11'$). These angular properties are, of course, very critical for the shape of the frozen solution spectrum of the paramagnetic complex. Neither eigenvalues nor eigenvectors of these hyperfine tensors were modified by the optimization program which simulated the experimental EPR spectrum; this confirms the excellent accord between EPR measurements and the calculated structure. The experimental $^{31}P-\tau_{\|}$ corresponds to a spin density of 0.12 in a p_π orbital of each phosphorus atom; the fact that the *odd* electron is located on the ligand is confirmed by the small anisotropy of the *g*-factor.

In $[Ni(bp)_2]^{\bullet-}$, the unpaired electron is totally delocalized on the ligands in a π^* orbital which is mainly constructed from the phosphorus p_π orbitals (DFT calculated *total* atomic spin density on each phosphorus atom: 0.185) and the carbon atoms C2, C2′, C12, C12′ involved in the inter-phosphinine bonds (total atomic spin densities on each of these carbons: 0.025). The SOMO obtained for the $(bp)^{\bullet-}$ anion are less affected by the chelation of nickel. As seen in Figure 6, this orbital remains bonding between the two phosphinine rings of the same ligand and antibonding between the phosphorus atoms and the adjacent central carbons (e.g., P1−C2, P1′−C2′). Accordingly, the reduction leads to an shortening of 0.023 Å of the C−C bridging bonds and an increase of 0.026 Å of the internal P−C bonds (e.g., P1−C2), whereas the Ni−P bond length increases only of 0.014 Å. The HDOMO in $[Ni(bp)_2]^{\bullet-}$ and the HOMO in $[Ni(bp)_2]$ are, of course, metal−ligand σ antibonding with a small participation of the $(MO)_{lp}$ mentioned above for the isolated ligand.

To have more information about the donor−acceptor interactions in the neutral complex $[Ni(bp)_2]$, we have used the charge decomposition analysis[21] method to calculate both the amount of ligand-to-metal charge donation (*d*) and metal-to-ligand back-donation (*b*). From the separation of $[Ni(bp)_2]$ into two fragments bp and Ni(bp), we found $d = 1.02$ and $b = 0.33$; the donation/back-donation ratio *d*/*b* is equal to 3.1. This ratio may be compared with the values of 2.1 found[24] for CO in $Ni(CO)_4$ and of 4.9 for the carbodiphosphorane ligand $C(PH_3)_2$ in $(CO)_3NiC(PH_3)_2$. This indicates that biphosphinine is a very good π-acceptor, even if the extent of "metal-to-ligand" back-donation is slightly smaller for each phosphorus of bp (0.165) than for CO (0.21).

It is worth mentioning that addition of an electron to bp makes the molecule more planar, whereas reduction of $[Ni(bp)_2]$ increases the PCCP dihedral angle of each ligand. This is probably due to synergic effect between σ-donation and back-bonding: in the reduced complex, the ligand π^* orbitals contain the unpaired electron and are less available for receiving electron from nickel; as seen above, a small increase in the PCCP torsion angle of the ligand decreases repulsion between the phosphorus lone pairs, diminishes σ-donation and consequently leads to smaller back-donation.

Concluding Remarks

Crystal structure, EPR/ENDOR spectroscopy, and DFT calculations have shown that one-electron reduction of biphos-

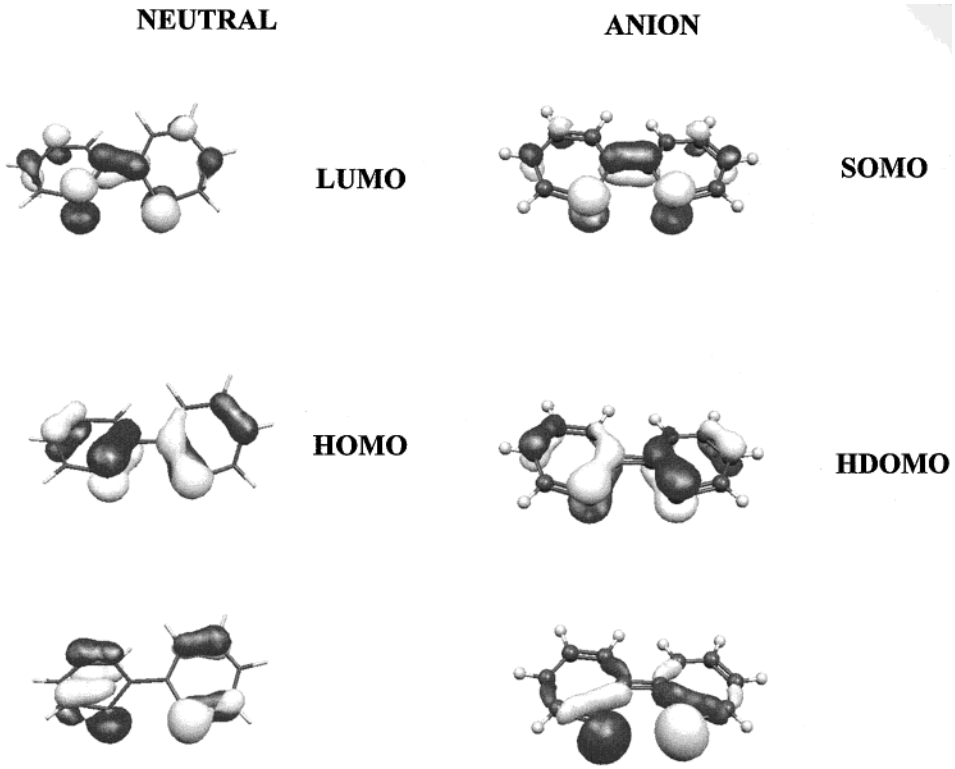

Figure 5. Frontier orbitals for bp and (bp)•⁻

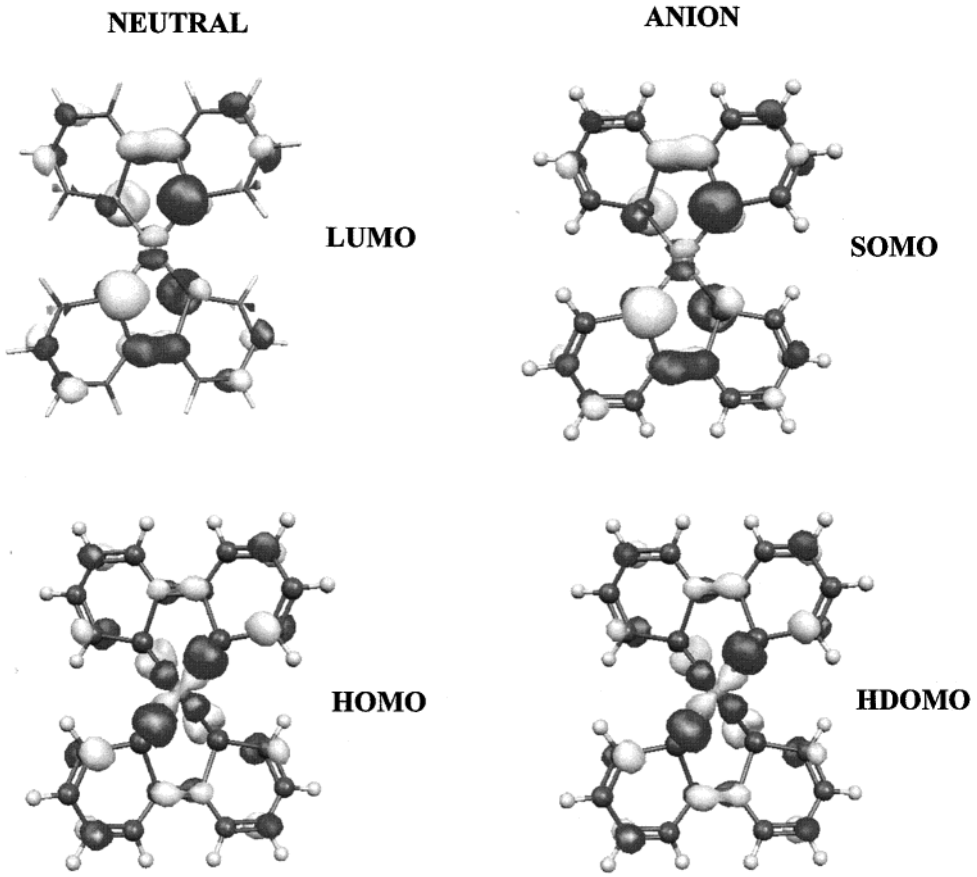

Figure 6. Frontier orbitals for [Ni(bp)$_2$] and [Ni(bp)$_2$]•⁻.

phinine provokes a drastic change in its molecular structure: the system becomes planar, the inter-phosphinine bond length is shortened; the unpaired electron is mainly delocalized in the P−C═C−P moiety in a π^* orbital characterized by a large participation of the phosphorus p orbitals. These properties make biphosphinine well-suited for stabilization of metals in a low oxidation state. This point was confirmed by adding an extra electron to [Ni$^{(0)}$(tmbp)$_2$] and by measuring the phosphorus hyperfine interactions. This first report on the structure of a 19-electron complex in which nickel is chelated by two ligands

containing unsaturated trivalent phosphorus atoms reveals how the neutral complex adapts its geometry to accommodate an extra electron. It illustrates the ability of phosphinine ligands to stabilize electron-rich transition metals and estimates, for $[Ni(bp)_2]$, the large contribution of π-back-donation to the Ni−biphosphinine bonding.

Acknowledgment. We thank the Swiss National Science Foundation for financial support as well as the CNRS and the Ecole Polytechnique (Palaiseau). Calculations were performed at the Swiss Center for Scientific Computing.

Supporting Information Available: Tables of crystal data, atomic coordinates and equivalent isotopic displacements parameters, bond lengths and angles, anisotropic displacements parameters, hydrogen coordinates and equivalent isotropic displacement parameters for [tmbp][Li(2.2.1)], table of geometrical parameters for $[Ni(bp)_2]$ and $[Ni(bp)_2]^{\bullet-}$ calculated by DFT by using the 6-31G* (neutral complex) and the 6-31+G* (anionic complex) basis sets for the ligand and the LANL2DZ basis set for the metal, and ENDOR spectrum (PDF). This material is available free of charge via the Internet at http://pubs.acs.org.

JA002125+